

Local-gauge finite-element method for electron waves in magnetic fields

Tsuyoshi Ueta^{1,*} and Yuu Miyagawa²¹*Physics Laboratory, The Jikei University School of Medicine, 8-3-1 Kokuryo-cho, Chofu, Tokyo, 182-8570, Japan*²*Graduate School of Science and Technology, Chiba University, 1-33 Yayoi-cho, Inage-ku, Chiba, 263-8522, Japan*

(Received 23 November 2011; published 15 August 2012)

The finite-element method (FEM) has already been extended to analyze transport properties of electron waves of two-dimensional electron systems in magnetic fields. Although many researchers have created new formulations or improvements to this method, few have analyzed how this method is applied to realistic systems. The present paper suggests that conventional formulations of the FEM do not give accurate results for large systems or for strong magnetic fields; in addition, it suggests that the selected gauge significantly influences the numerical results. Furthermore, this paper proposes a conceptually different formulation of the FEM that solves the poor convergence problem. This formulation is simple: matrix elements are multiplied by the Peierls phase in the absence of a magnetic field. To show the advantages of this formulation, numerical examples are presented.

DOI: [10.1103/PhysRevE.86.026707](https://doi.org/10.1103/PhysRevE.86.026707)

PACS number(s): 02.70.Dh, 73.23.-b

I. INTRODUCTION

In a two-dimensional electron system (2DES) formed in an insulator-semiconductor heterointerface, ballistic transport occurs, in which the mean free path exceeds the size of the device. To design a device that uses such an electron system, it is necessary to exactly analyze the behavior of electron waves within a system of complicated shape. Various approximations are applicable for diffusive electronic transport when electrons are repeatedly scattered within a system; however, no approximation is applicable for ballistic transport. Moreover, because a magnetic field is generally employed as one of the external control parameters in experiments, it is necessary to analyze the behavior of electron waves in a magnetic field [1].

The behavior of electron waves in a magnetic field has so far been analyzed using methods such as the mode-matching [2], finite-difference (FDM), tight-binding [1], finite-element (FEM) [3,4] and boundary-element (BEM) methods [4,5]. The BEM is most convenient for analyzing waves within a system having a complicated shape; therefore, it has been extended to include magnetic fields and has been applied to many problems [6,7].

It is, however, difficult to use the BEM to analyze cases with continuously varying potentials, spin-orbit interactions, or the Rashba effect [8]. The FEM can be used to analyze such cases. Furthermore, the FEM has been extended to include electron waves in a magnetic field by many researchers [9,10], and it is continuously being improved [11].

Many studies have formulated the FEM for electron waves in a magnetic field and investigated its simple applications. However, few studies have used this method to analyze physical phenomena [9] and characteristics of realistic devices.

When electron wave functions in a magnetic field are calculated using the FEM, the numerical solution depends on the gauge of the vector potential employed and the convergence is poor. These are the major reasons for the limited use of the FEM for such a purpose.

The present paper determines the origin of the gauge dependence and poor convergence, and it creates a different formulation of the FEM. Numerical results for the problem solved in Ref. [11] are shown as an example of the application of the FEM formulation proposed here, and the succinctness and superiority of this formulation are also elucidated.

II. USUAL FORMULATION OF THE FEM AND ITS PROBLEMS

We treat electrons within a semiconductor in terms of the effective mass model. When a vector potential $\mathbf{A}(\mathbf{r})$ is applied to an electron system, the wave function ψ of an electron wave generally obeys the Schrödinger equation

$$\frac{1}{2m}\{(-i\hbar\nabla - q\mathbf{A})^2 + V(\mathbf{r})\}\psi = E\psi, \quad (1)$$

where the quantities q , m , $V(\mathbf{r})$, and E represent the charge, effective mass, potential, and energy of an electron, respectively.

In a 2DES, electrons are confined in the thick direction; thus the momentum of an electron in this direction is quantized. The depth of a 2DES is so small that the quantum state in the direction perpendicular to the 2DES is in the ground state. Therefore, it is sufficient if we account for the motion of electrons in just two dimensions.

Assuming a 2DES in the xy plane and a uniform magnetic field of strength B applied along the positive direction of the z axis, the vector potential can be chosen as $\mathbf{A} = B(- (1-s)y, sx, 0)$. Here s is an arbitrary real number.

In the usual formulation, Eq. (1) in two dimensions is expanded as

$$\begin{aligned} & -\frac{\hbar^2}{2m}\nabla^2\psi + i\frac{qB\hbar}{m}\left\{-(1-s)y\frac{\partial\psi}{\partial x} + sx\frac{\partial\psi}{\partial y}\right\} \\ & + \frac{q^2B^2}{2m}\{(1-s)^2y^2 + s^2x^2\}\psi = \{E - V(\mathbf{r})\}\psi, \quad (2) \end{aligned}$$

and the second and third terms on the left-hand side are treated as potentials introduced by the magnetic field. That

*tsuyoshi_ueta@jikei.ac.jp

is, the potential is formulated in the same manner as an electromagnetic wave with a spatially varying wave number.

To define the terms referred to in the present formulation, we briefly summarize the usual formulation below. The domain to be analyzed is divided into smaller fractions (finite elements) of triangular or quadrangular shapes, and the coordinates of the j th vertex (node) are set to \mathbf{r}_j . In this study, we assume triangular elements.

A continuous real function of \mathbf{r} , which is 1 only at the j th node and 0 at all other nodes, linearly connects the nodes surrounding the j th node. It satisfies the condition

$$N_j(\mathbf{r}_k) = \begin{cases} 1, & j = k, \\ 0, & j \neq k, \end{cases} \quad (3)$$

and it is chosen as the shape (interpolation) function $N_j(\mathbf{r})$ for the j th node.

A wave function within the whole domain is expanded in terms of the shape function $N_j(\mathbf{r})$ as follows:

$$\psi(\mathbf{r}) = \sum_j N_j(\mathbf{r})\psi_j, \quad (4)$$

and it is employed as a trial function. From the variation of the functional

$$\mathcal{L} = \psi^\dagger (\mathbf{K} - \mathbf{M}) \psi - \psi^\dagger \mathbf{Q} \quad (5)$$

with respect to ψ^\dagger , we obtain simultaneous equations about $\{\psi_i\}$ as

$$(\mathbf{K} - \mathbf{M}) \psi = \mathbf{Q}, \quad (6)$$

where ψ is defined as a column vector of which the i th component is the wave function ψ_i at the i th node.

The matrices \mathbf{K} and \mathbf{M} , and the vector \mathbf{Q} are respectively defined as follows:

$$\mathbf{K}_{jk} = \int_{v_{jk}} \left(\frac{\partial N_j}{\partial x} \frac{\partial N_k}{\partial x} + \frac{\partial N_j}{\partial y} \frac{\partial N_k}{\partial y} \right) d\mathbf{r}, \quad (7)$$

$$\begin{aligned} \mathbf{M}_{jk} &= E \int_{v_{jk}} N_j N_k d\mathbf{r} \\ &- i \frac{qB\hbar}{m} \sum_l \left\{ -(1-s)y_k \int_{v_{jk}} N_j N_l \frac{\partial N_k}{\partial x} d\mathbf{r} \right. \\ &\left. + sx_k \int_{v_{jk}} N_j N_l \frac{\partial N_k}{\partial y} d\mathbf{r} \right\} \\ &- \sum_l \left[V(\mathbf{r}_l) + \frac{q^2 B^2}{2m} \{ (1-s)^2 y_l^2 + s^2 x_l^2 \} \right] \\ &\times \int_{v_{jk}} N_j N_k N_l d\mathbf{r}, \quad (8) \\ \mathbf{Q}_j &= \sum_k q(\mathbf{r}_k) \int_{S_N} N_j N_k dS. \quad (9) \end{aligned}$$

Here the subscript v_{jk} shows that the integration is performed over the element that has the j th and k th nodes as two vertices. \int_{S_N} is the integration over the boundary on which the value of the normal derivative of the wave function is given, and $q(\mathbf{r})$ is the normal derivative given on a portion of the boundary.

If we employ this formulation, the last term of matrix \mathbf{M} may become very large; thus, this term may quickly vary if

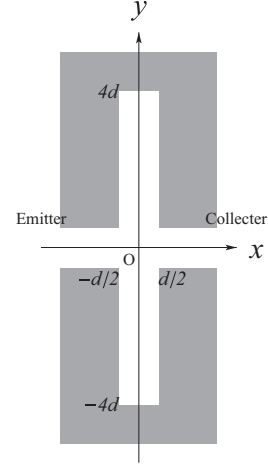


FIG. 1. Geometry of a cross-shaped waveguide.

the system size is large or if the magnetic field is strong, as already indicated for the simple FDM. The matrix \mathbf{M} depends on the gauge of the vector potential employed, i.e., on s . We have improved the formulation of the FEM such that the determined physical quantities (observables) are relatively independent of the gauge [11]. In Ref. [11], the eigenvalue problem of electron waves in a rectangular quantum cavity of width $2d$ and length d , in which the wave function was set to zero on the boundary, this problem was numerically analyzed for four different gauges of the vector potential. The authors presented the three lowest eigenvalues of the dimensionless wave number defined by $kd = \sqrt{2mE}d/\hbar$ for four different gauges (Table I of Ref. [11]). Furthermore, they stated that “the values of the energy levels converge at almost the same values independent of the vector potentials as the number of the quadratic triangular elements increases, so we confirm the invariance in the gauge transformation.” However, the third decimal place of the eigen wave numbers depends on the gauge, even for 1250 elements.

As an added example of computation that clearly shows gauge dependence [12], we consider the cross-junction structure shown in Fig. 1. It is a so-called rectangular quantum dot of width d and vertical length $8d$, to which an emitter and a collector of width d are attached to the left and right, respectively.

The boundary conditions on the emitter and the collector orifices are determined according to Sec. II B of Ref. [9]. Linear shape functions, namely, Lagrange functions for linear interpolation, are employed. For computational convenience, however, it is assumed that the emitter and collector portions are not subjected to a magnetic field, and the vector potentials within these portions are considered to be continuous with that within the region in which the magnetic field is applied.

Next, we set the vector potential within the cavity as $\mathbf{A} = (-By, 0, 0)$. When the fundamental transverse mode wave of $kd = 10$ is injected from the emitter, the transmissivity T and reflectivity R are calculated as functions of the number of nodes N_s for the magnetic field $\tilde{B} \equiv qBd^2/\hbar = 0-5$. The probability conservation law $T + R = 1$ must be satisfied in transport problems; therefore, this law is often employed as an indicator of calculation accuracy. In the computed results,

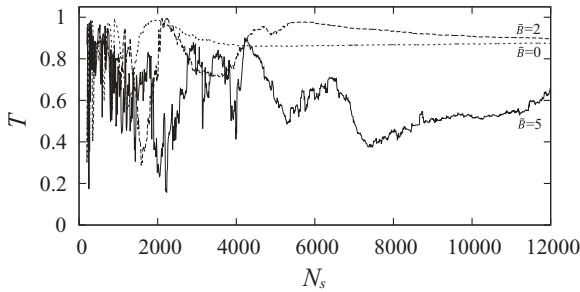


FIG. 2. Dependence of transmissivity T through the structure shown in Fig. 1 on the number of nodes N_s for $\tilde{B} = 0, 2$, and 5 . The fundamental transverse mode is injected from the emitter and the wave number is set as $Kd = 10$. Linear elements are employed.

the calculation error $|T + R - 1|$ is less than 0.02% for $N_s \geq 2000$.

The distance between the nearest neighbor nodes for $N_s = 3000$ is approximately $1/8$ the wavelength of $Kd = 10$; thus the convergence for $\tilde{B} = 0$ is reasonable. As shown in Fig. 2, however, the transmissivity T for $\tilde{B} = 0$ asymptotically converges to a definite value for $N_s \geq 3000$, whereas T for larger values of \tilde{B} hardly converges even when N_s is greater than 6000.

To investigate the reason for poor convergence in the presence of a magnetic field, the probability density $|\psi|^2$ and phase $\text{Im}(\ln \psi)$ of the wave function for $\tilde{B} = 20$ are shown in Fig. 3. In this case, the ratio of the cyclotron radius r_c to the width d of the emitter is $r_c/d = Kd/\tilde{B} = 0.5$; therefore, classical electron orbits predict that the probability density is expected to spread over the entire system. However, Fig. 3(a) shows that the probability density does not diffuse to the upper and lower ends of the system. The probability density does not vary quickly even for large $|y|$, whereas the phase varies quickly as $|y|$ increases. Such poor convergence in the presence of a magnetic field is attributed to not having enough finite elements to express the wave function accurately, because its phase varies quickly for large $|y|$.

Figures 4 and 5 show the numerical results for the vector potentials $\mathbf{A} = \frac{1}{2}B(-y, x, 0)$ and $\mathbf{A} = B(0, x, 0)$, respectively. For these cases, we employed quadratic finite elements. In the

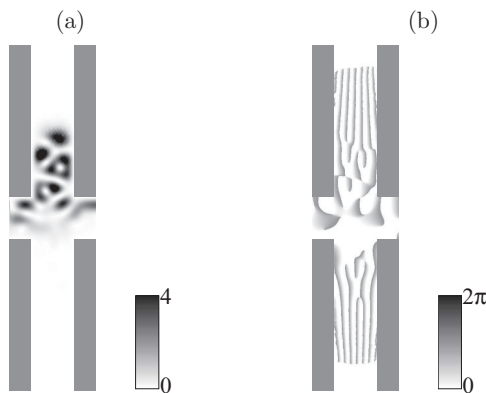


FIG. 3. Density plots of the probability density (a) and phase (b) of a wave function for $kd = 10$, $\tilde{B} = 20$, and $\mathbf{A} = (-By, 0, 0)$, which is a case of insufficient convergence. Quadratic elements are employed.

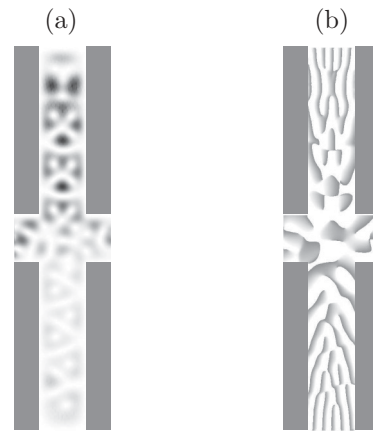


FIG. 4. Density plots of the probability density (a) and phase (b) for $kd = 10$, $\tilde{B} = 20$, and $\mathbf{A} = \frac{1}{2}B(-y, x, 0)$, which is also a case of insufficient convergence. Quadratic elements are employed.

case of $\mathbf{A} = B(0, x, 0)$, both the transmissivity and electron probability density agree with those calculated by the BEM with sufficient calculation accuracy. In Fig. 5(b), even if $|y|$ is large, the phase does not significantly oscillate. These results show that the rapid variation of the phase far from the origin of the vector potential results in poor convergence. Indeed, when the gauge of the vector potential is transformed from $\mathbf{A} = (0, Bx, 0)$ to $\mathbf{A} = (-By, 0, 0)$, the wave function is multiplied by a phase factor $\exp(-iqBxy/\hbar)$.

In that context, it is observed that $\mathbf{A} = (-By, 0, 0)$ is the most improper gauge to analyze this system. Because the phase factor does not appear in $|\psi|^2$, we cannot find such oscillation only by checking the probability density.

When a system extends in a certain direction, poor convergence can be avoided by choosing a suitable gauge. However, when a system is isotropic, such as a circle, and is large, poor convergence cannot be avoided using a global gauge transformation. Therefore, in the present paper, a conceptual formulation of the FEM that solves the poor convergence issue is proposed, and numerical examples are presented to show its validity, efficiency, and advantages.

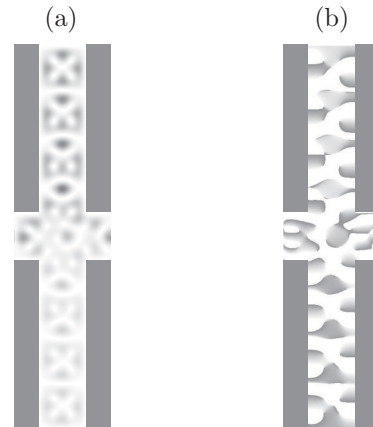


FIG. 5. Density plots of the probability density (a) and phase (b) for $kd = 10$, $\tilde{B} = 20$, and $\mathbf{A} = (0, Bx, 0)$. Quadratic elements are employed.

III. FORMULATION OF THE FEM USING THE MAGNETIC TRANSLATION OPERATOR

Let us consider the Schrödinger equation (1) near the origin for the symmetric gauge $\mathbf{A} = \frac{1}{2}\mathbf{B}(-y, x, 0)$. A wave function near the origin can be approximated by that in the absence of a magnetic field, because $\mathbf{A} \sim \mathbf{0}$ near the origin.

Here, we define the magnetic translation operator $T(\mathbf{R})$ [13] as

$$T(\mathbf{R}) \equiv \exp\left(\frac{i}{\hbar}\mathbf{R} \cdot (\mathbf{p} + q\mathbf{A})\right). \quad (10)$$

The operator $T(\mathbf{R})$ operates on an arbitrary function $f(\mathbf{r})$ as follows:

$$T(\mathbf{R})f(\mathbf{r}) = e^{-i(q/2\hbar)\mathbf{B} \cdot (\mathbf{R} \times \mathbf{r})} f(\mathbf{r} + \mathbf{R}), \quad (11)$$

such that it satisfies the following relations:

$$\begin{aligned} T(\mathbf{R})V(\mathbf{r})\phi(\mathbf{r}) &= e^{-i(q/2\hbar)\mathbf{B} \cdot (\mathbf{R} \times \mathbf{r})} V(\mathbf{r} + \mathbf{R})\phi(\mathbf{r} + \mathbf{R}) \\ &= V(\mathbf{r} + \mathbf{R})T(\mathbf{R})\phi(\mathbf{r}) \end{aligned} \quad (12)$$

and

$$[(\mathbf{p} - q\mathbf{A})^2, T(\mathbf{R})] = 0. \quad (13)$$

Here $[\cdot, \cdot]$ is the commutator defined by $[A, B] \equiv AB - BA$, and these relations are valid only for the symmetric gauge [13].

Applying the operator $T(\mathbf{R})$ to both sides of Eq. (1) near the origin, we obtain

$$\begin{aligned} T(\mathbf{R}) \left[\frac{1}{2m}(\mathbf{p} - q\mathbf{A})^2 + V(\mathbf{r}) \right] \psi(\mathbf{r}) \\ = \left[\frac{1}{2m}(\mathbf{p} - q\mathbf{A})^2 + V(\mathbf{r} + \mathbf{R}) \right] T(\mathbf{R})\psi(\mathbf{r}) \\ = ET(\mathbf{R})\psi(\mathbf{r}). \end{aligned} \quad (14)$$

Here the wave function

$$T(\mathbf{R})\psi(\mathbf{r}) = e^{-i(q/2\hbar)\mathbf{B} \cdot (\mathbf{R} \times \mathbf{r})} \psi(\mathbf{r} + \mathbf{R}) \quad (15)$$

is the one near the point $\mathbf{r} = -\mathbf{R}$ for the vector potential $\mathbf{A} = \frac{1}{2}\mathbf{B} \times (\mathbf{r} + \mathbf{R})$, which vanishes at $\mathbf{r} = -\mathbf{R}$. The wave function $\psi(\mathbf{r} + \mathbf{R})$ is the one near the point $\mathbf{r} = -\mathbf{R}$ for zero vector potential near the point $\mathbf{r} = -\mathbf{R}$.

Because $\psi_j N_j(\mathbf{r})$ satisfactorily approximates the wave function $\psi(\mathbf{r} - \mathbf{r}_j)$ near the point \mathbf{r}_j , the wave function for the entire system can be expressed as follows:

$$\psi(\mathbf{r}) = \sum_j \psi_j T(\mathbf{r}_j) N_0(\mathbf{r}) = \sum_j \psi_j e^{i(q/2\hbar)\mathbf{B} \cdot (\mathbf{r}_j \times \mathbf{r})} N_j(\mathbf{r}). \quad (16)$$

By applying the gauge-invariant kinetic energy operator to this wave function, we obtain

$$\begin{aligned} \frac{1}{2m}[\mathbf{p} - q\mathbf{A}(\mathbf{r})]^2 \psi(\mathbf{r}) \\ = \frac{1}{2m}[\mathbf{p} - q\mathbf{A}(\mathbf{r})]^2 \sum_j \psi_j e^{i(q/2\hbar)\mathbf{B} \cdot (\mathbf{r}_j \times \mathbf{r})} N_j(\mathbf{r}) \\ = \sum_j \psi_j e^{i(q/2\hbar)\mathbf{B} \cdot (\mathbf{r}_j \times \mathbf{r})} \frac{1}{2m} \{ \mathbf{p} - q[\mathbf{A}(\mathbf{r}) - \mathbf{A}(\mathbf{r}_j)] \}^2 N_j(\mathbf{r}) \\ \approx \sum_j \psi_j e^{i(q/2\hbar)\mathbf{B} \cdot (\mathbf{r}_j \times \mathbf{r})} \frac{1}{2m} \mathbf{p}^2 N_j(\mathbf{r}). \end{aligned} \quad (17)$$

Thus, if we expand the wave function as Eq. (16), the approximate vector potential need not be considered. The phase factor attached to the shape function transforms the local gauge to the original global gauge: $\mathbf{A} = \frac{1}{2}\mathbf{B} \times \mathbf{r}$.

Omitting the term of the Neumann boundary condition for simplicity, we obtain the functional for the calculus of variations as follows:

$$\begin{aligned} \mathcal{L} = \int_V \left[\frac{1}{2m} \{ (\mathbf{p} - q\mathbf{A})\psi \}^* \cdot \{ (\mathbf{p} - q\mathbf{A})\psi \} \right. \\ \left. - \psi^* [E - V(\mathbf{r})] \psi \right] d\mathbf{r}. \end{aligned}$$

$$\begin{aligned} \text{The first term} &= \frac{1}{2m} \sum_{j,k} \psi_j^* \int_V \{ e^{i(q/2\hbar)\mathbf{B} \cdot (\mathbf{r}_j \times \mathbf{r})} \mathbf{p} N_j(\mathbf{r}) \}^* \\ &\quad \cdot \{ e^{i(q/2\hbar)\mathbf{B} \cdot (\mathbf{r}_k \times \mathbf{r})} \mathbf{p} N_k(\mathbf{r}) \} d\mathbf{r} \psi_k \\ &= -\frac{\hbar^2}{2m} \sum_{j,k} \psi_j^* \int_{V_{jk}} e^{i(q/2\hbar)\mathbf{B} \cdot \{ (\mathbf{r}_k - \mathbf{r}_j) \times \mathbf{r} \}} \\ &\quad \times [\nabla N_j(\mathbf{r})] \cdot [\nabla N_k(\mathbf{r})] d\mathbf{r} \psi_k. \end{aligned}$$

$$\begin{aligned} \text{The second term} &= E \sum_{j,k} \psi_j^* \int_V \{ e^{i(q/2\hbar)\mathbf{B} \cdot (\mathbf{r}_j \times \mathbf{r})} N_j(\mathbf{r}) \}^* \\ &\quad \times \{ e^{i(q/2\hbar)\mathbf{B} \cdot (\mathbf{r}_k \times \mathbf{r})} N_k(\mathbf{r}) \} d\mathbf{r} \psi_k \\ &= E \sum_{j,k} \psi_j^* \int_{V_{jk}} e^{i(q/2\hbar)\mathbf{B} \cdot \{ (\mathbf{r}_k - \mathbf{r}_j) \times \mathbf{r} \}} \\ &\quad \times N_j(\mathbf{r}) N_k(\mathbf{r}) d\mathbf{r} \psi_k. \end{aligned}$$

$$\begin{aligned} \text{The third term} &= \sum_{j,k} \psi_j^* \int_V \{ e^{i(q/2\hbar)\mathbf{B} \cdot (\mathbf{r}_j \times \mathbf{r})} N_j(\mathbf{r}) \}^* \\ &\quad \times \left(\sum_l V_l N_l(\mathbf{r}) \right) \\ &\quad \times \{ e^{i(q/2\hbar)\mathbf{B} \cdot (\mathbf{r}_k \times \mathbf{r})} N_k(\mathbf{r}) \} d\mathbf{r} \psi_k \\ &= \sum_{j,k,l} V_l \psi_j^* \int_{V_{jk}} e^{i(q/2\hbar)\mathbf{B} \cdot \{ (\mathbf{r}_k - \mathbf{r}_j) \times \mathbf{r} \}} \\ &\quad \times N_j(\mathbf{r}) N_l(\mathbf{r}) N_k(\mathbf{r}) d\mathbf{r} \psi_k. \end{aligned}$$

Here $\int_{V_{jk}} d\mathbf{r}$ is the volume integration in the triangular finite element that has two vertices at \mathbf{r}_j and \mathbf{r}_k . By introducing a new integration variable $\boldsymbol{\xi}$ defined by $\mathbf{r} = \mathbf{r}_k + \boldsymbol{\xi}$, the matrix element \mathbf{K}_{jk} can be written as follows:

$$\begin{aligned} \mathbf{K}_{jk} &\equiv -\frac{\hbar^2}{2m} \int_{V_{jk}} e^{i(q/2\hbar)\mathbf{B} \cdot \{ (\mathbf{r}_k - \mathbf{r}_j) \times (\mathbf{r}_k + \boldsymbol{\xi}) \}} \\ &\quad \times [\nabla N_j(\boldsymbol{\xi})] \cdot [\nabla N_k(\boldsymbol{\xi})] d\boldsymbol{\xi} \\ &= e^{i(q/2\hbar)\mathbf{B} \cdot (\mathbf{r}_k \times \mathbf{r}_j)} \left(-\frac{\hbar^2}{2m} \right) \\ &\quad \times \int_{V_{jk}} e^{i(q/2\hbar)\mathbf{B} \cdot \{ (\mathbf{r}_k - \mathbf{r}_j) \times \boldsymbol{\xi} \}} [\nabla N_j(\boldsymbol{\xi})] \cdot [\nabla N_k(\boldsymbol{\xi})] d\boldsymbol{\xi} \\ &\approx e^{i(q/2\hbar)\mathbf{B} \cdot (\mathbf{r}_k \times \mathbf{r}_j)} \left(-\frac{\hbar^2}{2m} \right) \int_{V_{jk}} (\nabla N_j) \cdot (\nabla N_k) d\boldsymbol{\xi} \\ &= e^{i(q/2\hbar)\mathbf{B} \cdot (\mathbf{r}_k \times \mathbf{r}_j)} \mathbf{K}_{jk}^0, \end{aligned} \quad (18)$$

where \mathbf{K}_{jk}^0 is the corresponding matrix element in the absence of a magnetic field. During the modification from the second

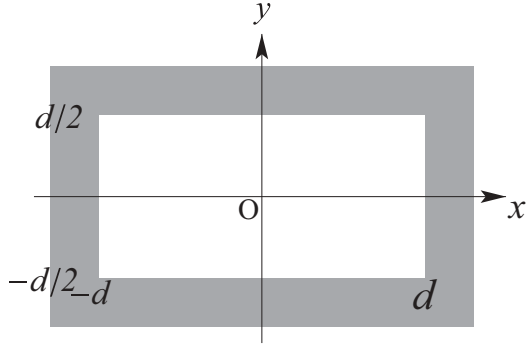


FIG. 6. Rectangular quantum cavity investigated in Ref. [11].

line to the third line, the phase factor in the integration is approximated as unity, assuming that the magnetic flux through any finite element is sufficiently less than the flux quantum h/q .

Similarly, we obtain

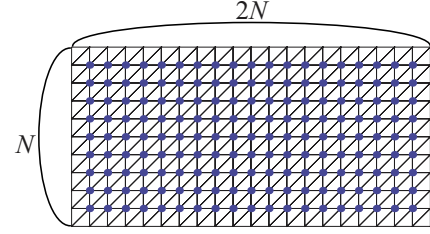
$$\begin{aligned} M_{jk} &\equiv \int_{V_{jk}} e^{i(q/2\hbar)\mathbf{B}\cdot(\mathbf{r}_k-\mathbf{r}_j)\times\mathbf{r}} \left\{ EN_j(\mathbf{r})N_k(\mathbf{r}) \right. \\ &\quad \left. - N_j(\mathbf{r}) \left(\sum_l V(\mathbf{r}_l)N_l(\mathbf{r}) \right) N_k(\mathbf{r}) \right\} d\mathbf{r} \\ &\approx e^{i(q/2\hbar)\mathbf{B}\cdot(\mathbf{r}_k\times\mathbf{r}_j)} M_{jk}^0. \end{aligned} \quad (19)$$

Note that the FEM for electron waves in a magnetic field can be approximately formulated only by multiplying the so-called Peierls phase factor with the matrices in the absence of a magnetic field. This is analogous to the tight-binding approximation (equivalent to the finite-difference approximation [1]) of the Schrödinger equation for electron waves in a magnetic field, which was derived by Peierls [14].

For $\mathbf{A} = \frac{1}{2}\mathbf{B}(-y, x, 0)$, the phase factor in Eqs. (18) and (19) is written as

$$e^{i(q/2\hbar)\mathbf{B}\cdot(\mathbf{r}_k\times\mathbf{r}_j)} = \exp \left[i \frac{q}{\hbar} \int_{\mathbf{r}_k}^{\mathbf{r}_j} \mathbf{A}(\mathbf{r}) \cdot d\mathbf{r} \right], \quad (20)$$

in which the arrow on the integral symbol indicates that integration is performed along the straight path from the point


 FIG. 7. (Color online) Finite elements: mesh in the rectangular quantum cavity for $N = 10$. The number of nodes (shown by dots) is given by $(N - 1) \times (2N - 1)$.

\mathbf{r}_k to \mathbf{r}_j [6]. The expression on the right-hand side is valid for arbitrary gauges satisfying $\text{rot}\mathbf{A} = (0, 0, B)$; therefore, the following equations are realized:

$$\mathbf{K}_{jk} = \exp \left[i \frac{q}{\hbar} \int_{\mathbf{r}_k}^{\mathbf{r}_j} \mathbf{A}(\mathbf{r}) \cdot d\mathbf{r} \right] \mathbf{K}_{jk}^0, \quad (21)$$

$$\mathbf{M}_{jk} = \exp \left[i \frac{q}{\hbar} \int_{\mathbf{r}_k}^{\mathbf{r}_j} \mathbf{A}(\mathbf{r}) \cdot d\mathbf{r} \right] \mathbf{M}_{jk}^0. \quad (22)$$

IV. NUMERICAL RESULTS

Here examples of numerical computations that use Eqs. (21) and (22) are shown. The numerical implementation is according to that specified in Refs. [9] and [12]. Again, linear finite elements are employed here.

A. Eigenvalue problem

To confirm the approximation accuracy and the gauge invariance of the solutions for the proposed method, we first analyze the eigenvalue problem within the rectangular quantum cavity shown in Fig. 6, which was analyzed in Ref. [11].

We discretize the system into triangular finite elements in order to divide a side of length d into N segments, as shown in Fig. 7. The system is analyzed for three types of gauge: $\mathbf{A} = B(-y, x, 0)/2$ [gauge 1, (d) of Ref. [11]], $B(-y, 0, 0)$ [gauge 2, (a)], and $B(0, x, 0)$ [gauge 3, (c)].

 TABLE I. Variations in the three lowest eigen wave numbers kd for three gauges, where N is the number of divisions of the side of width d . The results determined by the tight-binding model are also shown.

Gauge	$N = 20$	$N = 90$	Ref. [11] Table I	Tight-binding model ($N = 20$)
		$k_0 d$		
1	5.079220411952475	5.069960104361848	5.070	5.01039
2	5.079220411952162	5.069960104429902	5.070	5.01039
3	5.079220411952306	5.069960104324939	5.071	5.01039
		$k_1 d$		
1	5.2358151469960035	5.223904279178192	5.224	5.09256
2	5.235815146996086	5.223904279230286	5.223	5.09256
3	5.235815146996177	5.223904279183718	5.228	5.09256
		$k_2 d$		
1	5.5357147392872115	5.519976451342494	5.520	5.27081
2	5.535714739287768	5.519976451347637	5.520	5.27081
3	5.535714739287288	5.51997645137805	5.528	5.27081

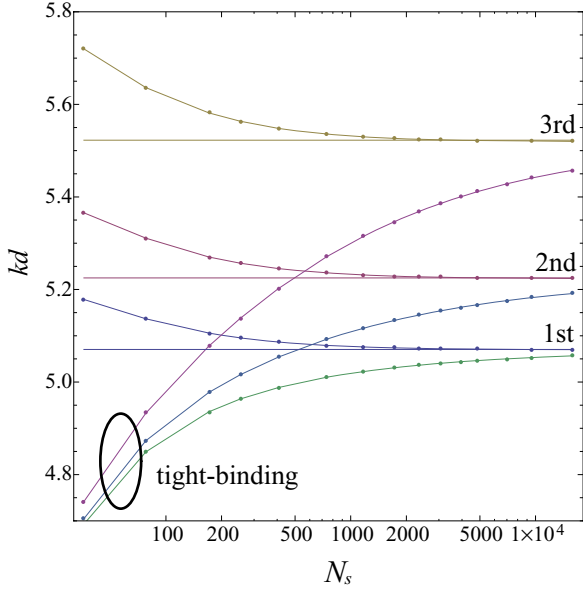


FIG. 8. (Color online) Variation of the three lowest eigen wave numbers kd_0 , kd_1 , and kd_2 as a function of the number of nodes N_s . Results computed with the tight-binding model are also shown. The three horizontal lines indicate the eigenvalues of Ref. [11] for “gauge 3.”

For $N = 20$ (1600 elements), the values of the three lowest eigen wave numbers (k_0d , k_1d , and k_2d) are shown in Table I with the results for the case of 1250 elements from Ref. [11]. Table I shows that the numerical results for any gauge determined by this method agree with 13 decimal places in calculation accuracy. This is also true for other numbers of divisions N and for the tight-binding model.

Note that the eigenvalues for $N = 20$ do not sufficiently converge; however, those for $N = 90$ converge.

The N_s dependence of the three lowest eigen wave numbers for “gauge 1” is shown in Fig. 8, in which the number of nodes N_s is given by $N_s = (N - 1) \times (2N - 1)$. The three horizontal lines in the figure indicate the three lowest eigenvalues in Ref. [11] for “gauge 3.” Each of them immediately and monotonically converges as the number of nodes increases.

In Fig. 8, the results computed using the tight-binding model are also plotted. This figure clearly shows that the proposed FEM converges much faster than the tight-binding model.

Figure 9 is a density plot of the probability density of $kd = 10.0247$ (the ninth eigen wave number) for $\tilde{B} = 100$ (i.e., the

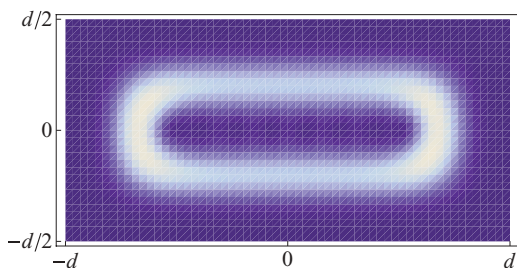


FIG. 9. (Color online) Density plot of the probability density of the ninth energy level ($kd = 10.0247$) for $\tilde{B} = 100$ and $N = 30$.

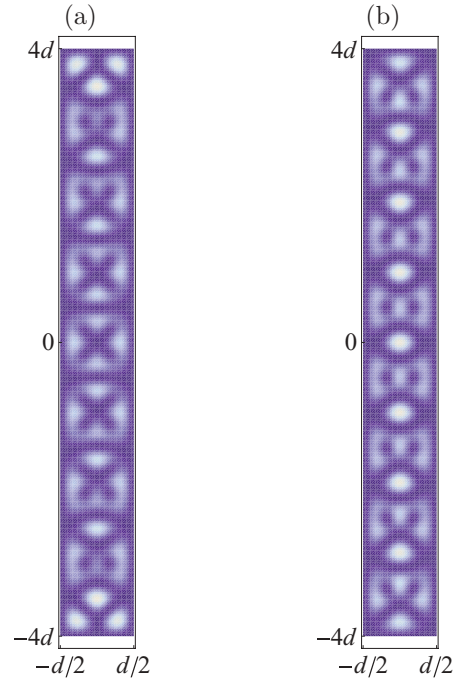


FIG. 10. (Color online) Density plots of the probability density for the two eigenstates $kd = 10.0159$ (a) and $kd = 9.95098$ (b) within an $8d \times d$ rectangular cavity for $\tilde{B} = 20$ and $N = 30$.

same value as that in Fig. 4 of Ref. [11]), as an example of a high-magnetic-field case. Despite using the approximate formulas given in Eqs. (21) and (22), which are valid for weak magnetic fields, the probability density in Fig. 9 agrees well with that in Fig. 4 of Ref. [11], even for a high magnetic field.

Next, we analyze a system with strong anisotropy and solve its energy eigenvalue problem. This system is a rectangular quantum cavity of length $8d$ and of width d , and it is the same as that in Fig. 1 except for the two waveguides. Even in this case, the numerical results are gauge invariant to the limit of computational accuracy.

Then, the case of gauge $\mathbf{A} = (-By, 0, 0)$, which is the most unfavorable in Fig. 3, is considered. For $\tilde{B} = 20$, the probability densities of the two energy eigenstates of $kd = 10.0159$ and 9.95098 nearest to $kd = 10$ employed in the transport problem in Sec. II, are shown in Fig. 10. The number of divisions N is set to $N = 30$.

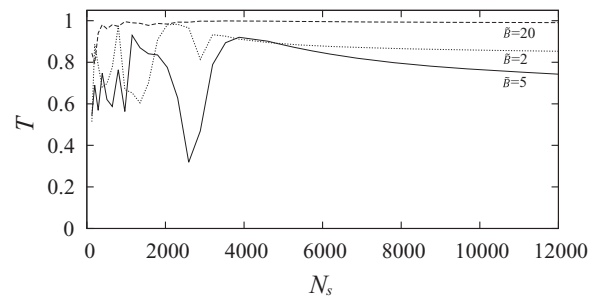


FIG. 11. Dependence of transmissivity T on the number of nodes N_s for $\tilde{B} = 2, 5$, and 20 . The fundamental mode is injected from the emitter, and the wave number is set to $Kd = 10$.

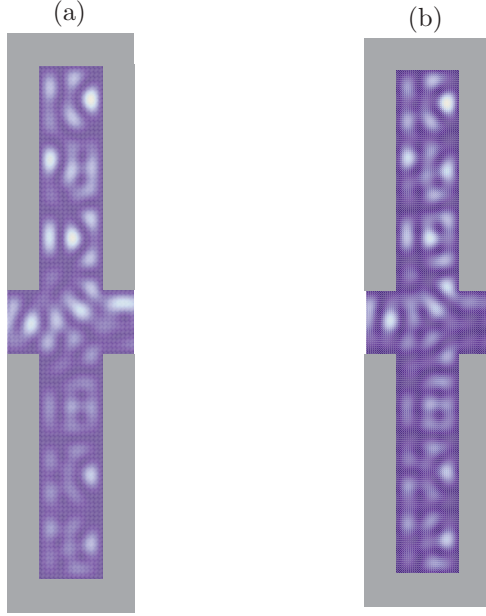


FIG. 12. (Color online) Density plots of the probability density for $\tilde{B} = 5$ determined by the present method (a) and by the BEM [6,7] (b) for the system shown in Fig. 1. The fundamental mode is injected from the emitter, and the wave number is set to $kd = 10$.

The probability density is distributed over the quantum cavity, and it does not give a result similar to that in Fig. 3. It turns out that the state originating from the eigenstate of $kd = 9.95098$ is excited in Fig. 5.

B. Electron-transport problems

The original motivation for this paper was the transport-related problem shown in Sec. II. Now, we consider the system shown in Fig. 1.

The dependence of the transmissivity T on the number of nodes N_s for $\tilde{B} = 2, 5$, and 20 is shown in Fig. 11. Linear elements are employed, and the gauge is set to $\mathbf{A} = (-By, 0, 0)$. For $N_s \geq 4000$, all the curves monotonically converge, although the curve of $\tilde{B} = 5$ in Fig. 2 does not show a smooth behavior up to $N_s = 12000$.

The density plot of the probability density for $\tilde{B} = 5$ is shown in Fig. 12(a), and the corresponding numerical result determined by the BEM [7] is shown in Fig. 12(b). Although the transmissivity does not sufficiently converge in the case of $\tilde{B} = 5$, the pattern of probability density determined by the proposed method agrees well with that determined by the BEM.

V. CONCLUSIONS

Considering the commutation relation between the magnetic translation operator and the gauge-invariant kinetic energy operator associated with the vector potential, the shape function is locally gauge transformed, so that the vector potential vanishes at the node where the shape function has a peak. The wave function has been expanded in terms of shape functions.

This expanded wave function has been used to formulate the FEM to account for the effect of a magnetic field only by inserting a phase factor. The method developed in this study has been applied to sample eigenvalue problems, and it has been shown that the method gives identical solutions within the calculation accuracy for any gauge.

It has been confirmed that the proposed method is practical, useful, and enables us to easily introduce a magnetic field to electron-transport problems. Moreover, for transport-related problems, the proposed method has the advantage that we can choose a gauge that eases the treatment of wave guides regardless of the shape of the system.

The approximation used in Eqs. (18) and (19) is the same as that in Peierls' tight-binding model in a magnetic field [1,14]; therefore, it is natural to compare the proposed method and the tight-binding model. Numerical results for the eigenvalue problem in Fig. 6 have been compared in Table I and Fig. 8. Assuming the same number of nodes, it has been confirmed that the calculation error of the FEM is less than $\sim 1/3$ of that of the tight-binding model (or the FDM); this error is the same as that in the absence of a magnetic field. The FEM could be used to analyze electron waves in magnetic fields in various research fields from now on.

Convergence in the presence of a finite magnetic field is slower than that in its absence as shown by the curves in Fig. 8 and the long tail of transmissivity in Fig. 11. This slow convergence is attributed to the approximation of setting the phase factor in the volume integration over a finite element to unity. The approximation accuracy systematically improves as the sizes of the finite elements decrease; however, when the approximation seriously affects the calculation accuracy, we may expand the phase factor in terms of a shape function like a potential; e.g.,

$$e^{i(q/2\hbar)\mathbf{B}\cdot(\mathbf{r}_k-\mathbf{r}_j)\times\xi} = \sum_l e^{i(q/2\hbar)\mathbf{B}\cdot\{(\mathbf{r}_k-\mathbf{r}_j)\times\mathbf{r}_l\}} N_l(\xi),$$

and perform volume integration over a finite element. In this case, the matrices \mathbf{K} and \mathbf{M} are given as follows:

$$\mathbf{K}_{jk} = e^{i(q/2\hbar)\mathbf{B}\cdot(\mathbf{r}_k\times\mathbf{r}_j)} \left(-\frac{\hbar^2}{2m} \right) \sum_l e^{i(q/2\hbar)\mathbf{B}\cdot\{(\mathbf{r}_k-\mathbf{r}_j)\times\mathbf{r}_l\}} \times \int_{V_{jk}} [\nabla N_j(\xi)] \cdot [\nabla N_k(\xi)] N_l(\xi) d\xi, \quad (23)$$

$$\mathbf{M}_{jk} = e^{i(q/2\hbar)\mathbf{B}\cdot(\mathbf{r}_k\times\mathbf{r}_j)} \sum_n e^{i(q/2\hbar)\mathbf{B}\cdot\{(\mathbf{r}_k-\mathbf{r}_j)\times\mathbf{r}_n\}} \times \int_{V_{jk}} \left\{ EN_j(\mathbf{r})N_k(\mathbf{r})N_n(\mathbf{r}) - \sum_l V(\mathbf{r}_l)N_j(\mathbf{r})N_l(\mathbf{r})N_k(\mathbf{r})N_n(\mathbf{r}) \right\} d\mathbf{r}. \quad (24)$$

Furthermore, we may employ the usual formulation of the FEM in magnetic fields, i.e., Eqs. (7)–(9) within a finite element for a local gauge. This is an exact formulation of the FEM.

- [1] Supriyo Datta, *Electronic Transport in Mesoscopic Systems* (Cambridge University Press, Cambridge, 1997).
- [2] R. L. Schult, H. W. Wyld, and D. G. Ravenhall, *Phys. Rev. B* **41**, 12760 (1990).
- [3] Craig S. Lent and David J. Kirkner, *J. Appl. Phys.* **67**, 6353 (1990).
- [4] L. Ramdas Ram-Mohan, *Finite Element and Boundary Element Applications in Quantum Mechanics* (Oxford University Press, Oxford, 2002).
- [5] H. R. Frohne, M. J. Mc Lennan, and S. Datta, *J. Appl. Phys.* **66**, 2699 (1989).
- [6] Tsuyoshi Ueta, *J. Phys. Soc. Jpn.* **61**, 4314 (1992).
- [7] Tsuyoshi Ueta, *Eng. Anal. Boundary Elements* **17**, 69 (1996).
- [8] Y. A. Bychkov and E. I. Rashba, *J. Phys. C* **17**, 6039 (1984).
- [9] Yongjiang Wang, Jian Wang, and Hong Guo, *Phys. Rev. B* **49**, 1928 (1994).
- [10] Manhua Leng and Craig S. Lent, *J. Appl. Phys.* **76**, 2240 (1994).
- [11] Koichi Hirayama, Yasuhiro Honma, Yoshio Hayashi, and Masanori Koshiba, *IEEE Photonics Technol. Lett.* **10**, 1359 (1998).
- [12] Yuu Miyagawa, Ph.D. thesis, Chiba University, 2008 (in Japanese).
- [13] E. Brown, *Phys. Rev.* **133**, A1038 (1964).
- [14] R. E. Peierls, *Z. Phys.* **80**, 763 (1933).